J|A|C|S COMMUNICATIONS

Published on Web 12/22/2009

Fe_xO_y@C Spheres as an Excellent Catalyst for Fischer−Tropsch Synthesis

Guobin Yu,[†] Bo Sun,[†] Yan Pei,[†] Songhai Xie,[†] Shirun Yan,[†] Minghua Qiao,*[,†] Kangnian Fan,[†] Xiaoxin Zhang,[‡] and Baoning Zong*[,‡]

Department of Chemistry and Shanghai Key Laboratory of Molecular Catalysis and Innovative Materials, Fudan University, Shanghai 200433, P. R. China, and State Key Laboratory of Catalytic Materials and Chemical Engineering, Research Institute of Petroleum Processing, SINOPEC, Beijing 100083, P. R. China

Received August 4, 2009; E-mail: mhqiao@fudan.edu.cn; zongbn@ripp-sinopec.com

When saccharides such as glucose, sucrose, and starch are hydrothermally treated at 160−200 °C, carbonaceous spheres with smooth surfaces and tunable sizes in the nano- to micrometer range are formed.[1,2] The saccharide molecules undergo dehydration and subsequent aromatization during the preparation, resulting in carbonaceous spheres featuring a hydrophobic core and a hydrophilic shell abundant in OH and C═O groups.[1] Templating these carbonaceous spheres or coupling with their formation process enables the synthesis of a variety of core−shell materials with diversified structures.[1,3,4] However, the synthesis of metal oxide−C hybrid materials with metal oxide nanocrystals encapsulated and highly dispersed in the carbonaceous spheres, which may find important applications in the development of high-performance sensors, adsorbents, and catalysts, remains a great challenge.

Since (i) iron nitrate can be transformed to iron oxide during the hydrothermal treatment,[5] (ii) iron oxide nanoparticles are expected to be more reluctant than metal nanoparticles to form large aggregates because metal oxides are covalently rather than metallically bonded, and (iii) iron oxide nanoparticles may tend to bind with the surface functional groups on carbon colloids derived from glucose through the Coulombic interaction,[6] we designed a one-pot hydrothermal cohydrolysis−carbonization process using glucose and iron nitrate as starting materials and succeeded in the fabrication of carbonaceous spheres embedded with highly dispersed iron oxide nanoparticles (designated as Fe_xO_y@C). Because of the confinement of the carbonaceous matter on metal oxide nanoparticles, materials with this interesting structure are promising functional materials in applications where the size of nanoparticles is crucial for their electronic, optical, and catalytic performance,[7] including the Fischer−Tropsch synthesis (FTS) investigated here.[8,9]

Figure 1 presents scanning electron microscopy (SEM) images of Fe_xO_y@C spheres with an iron nitrate/glucose nominal molar ratio of 3/5 (based on carbon) prepared by hydrothermal treatment at 80 °C for 24 h. The as-prepared sample contains particles with perfect spherical shape, a narrow size distribution of ∼6 μm, and a smooth surface. In contrast, no carbonaceous spheres were observed below 140 °C in the absence of iron nitrate.[1] The drastic reduction in the hydrothermal temperature is attributed to the ability of the metal salt or metal oxide to catalyze the dehydration of saccharides.[10] In fact, iron nitrate is so efficient in catalyzing the carbonization of glucose that Fe_xO_y@C spheres emerged after as little as 2 h of hydrothermal treatment at 80 °C. The SEM image of crushed Fe_xO_y@C spheres (Figure 1d) reveals the solid rather than hollow interior. Moreover, the layered structure disclosed in Figure 1d implies a layer-by-layer (LBL) growth mode during the formation of the Fe_xO_y@C spheres.

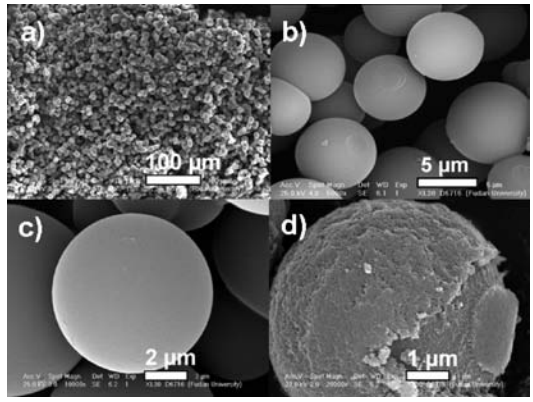

Figure 1. (a−c) SEM images of the Fe_xO_y@C spheres at different magnifications. (d) SEM image of a crushed Fe_xO_y@C sphere.

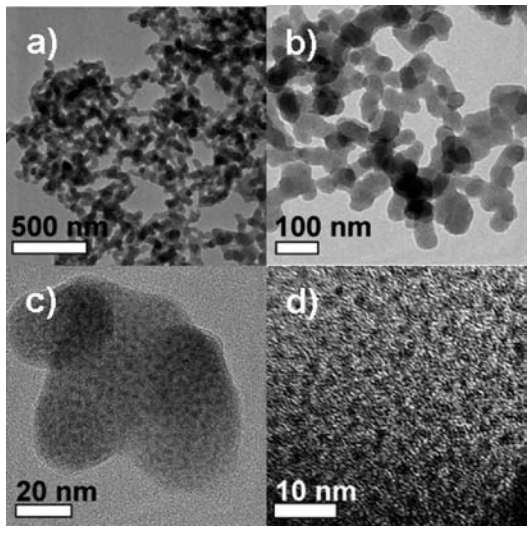

Figure 2. (a−c) TEM images of ground Fe_xO_y@C spheres at different magnifications, showing cross-linked nanorods inside. (d) HRTEM image of one carbonaceous nanorod embedded with iron oxide nanoparticles.

In order to unveil the microstructure of the Fe_xO_y@C spheres, the sample was ground and characterized by transmission electron microscopy (TEM). The images in Figure 2a−c show that the Fe_xO_y@C spheres are constructed of nanorods with a small length-to-diameter aspect ratio of ∼3 that are interconnected in three dimensions. The high-resolution TEM (HRTEM) image of one nanorod is shown in Figure 2d, which demonstrates the homogeneous distribution of darker nanoparticles with diameter of ∼1 nm in a matrix with a lower contrast. Since energy-dispersive X-ray (EDX) analysis confirmed the coexistence of iron and carbon in

[†] Fudan University.
[‡] SINOPEC.

10.1021/ja906370b

the sample and the electron density of iron is higher than that of carbon, the nanoparticles in Figure 2d are related to iron while the matrix is ascribed to the carbonaceous matter. Because the iron species are too small for the phase composition to be ascertained by TEM or X-ray diffraction, the ^{57}Fe Mössbauer spectrum of the sample was acquired (Figure 3a). The spectrum can be resolved into two quadrupole doublets, one with isomer shift (IS) and quadrupole splitting (QS) values of 1.21 mm s^{-1} and 1.81 mm s^{-1}, respectively, and the other with IS = 0.38 mm s^{-1} and QS = 0.91 mm s^{-1}. The former is ascribable to a high-spin Fe(II) center in an oxygen-rich coordination environment and the latter to a high-spin Fe(III) center.[11] This ascription was further validated by X-ray absorption spectroscopy (XAS), from which the Fe K-edge energy of the Fe_xO_y@C spheres (7121.3 eV) was found to be between those of FeO and Fe_3O_4 and far from those of Fe foil and Fe_2O_3 (Figure S1 and Table S1 in the Supporting Information). The areas under the fitted curves in Figure 3a gave an estimated value of 0.811: 0.189 for the Fe(II)/Fe(III) atomic ratio.

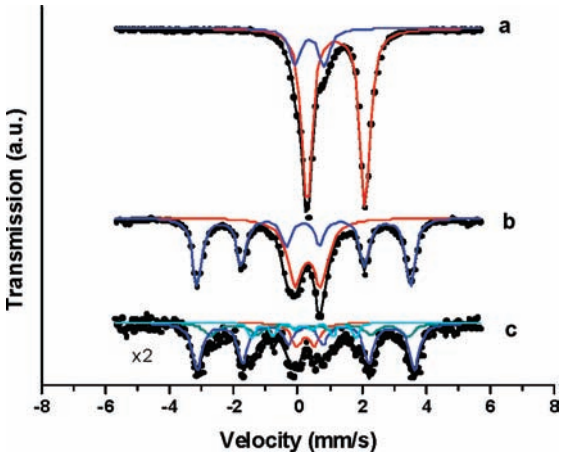

Figure 3. ^{57}Fe Mössbauer spectra of (a) the as-prepared Fe_xO_y@C spheres, recorded at 25 °C; (b) Fe_xO_y@C spheres reduced by 5% H_2/Ar at 400 °C for 16 h, recorded at 25 °C; and (c) sample (b), recorded at −258 °C. The computer fits are shown as solid lines.

Scheme 1. Illustration of the Formation Process of the Fe_xO_y@C Spheres[a]

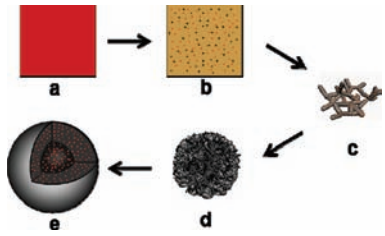

[a] (a) Aqueous solution containing glucose and iron nitrate. (b) Carbonaceous colloids (black dots) and iron oxide nanoparticles (red dots) generated at the initial stage of the hydrothermal treatment. (c) Carbonaceous nanorods with embedded iron oxide nanoparticles. (d) Large aggregate from further polymerization of the nanorods. (e) Fe_xO_y@C sphere with iron oxide nanoparticles highly dispersed inside.

On the basis of these characterizations, the formation process of the Fe_xO_y@C spheres with Fe_xO_y nanoparticles embedded in the carbonaceous matrix is illustrated in Scheme 1. We postulate that iron nitrate catalyzes the dehydration of glucose at the initial stage of the synthesis, leading to small carbonaceous colloids with a low degree of polymerization. Meanwhile, iron nitrate is transformed to FeOOH under the hydrothermal conditions[5] and further reduced to Fe_xO_y by hydrogen released from the carbonization process.[12] The Fe_xO_y nanoparticles then combine with small carbonaceous colloids through Coulombic interactions with the surface functional groups (i.e., OH and C═O) and condense to form Fe_xO_y-in-C nanorods, which are self-assembled to Fe_xO_y@C spheres via further intermolecular dehydration of the surface functional groups following the LBL mechanism. The homogeneous distribution of the Fe_xO_y nanoparticles in the carbonaceous spheres as revealed by HRTEM strongly indicates the good coupling between the formation of Fe_xO_y nanoparticles and the formation of small carbonaceous colloids; otherwise, isolated iron oxide particles and carbonaceous spheres or iron oxide−carbon core−shell spheres would be expected.

Since Fe_xO_y nanoparticles are formed and encapsulated during the formation of the carbonaceous spheres, the loading of iron oxide is substantially higher than that prepared by other methods utilizing only the surface OH and C═O functionalities of the carbonaceous spheres. It was determined by chemical analysis that the loading of iron oxide calculated in terms of Fe_2O_3 could be as high as 22 wt % for the Fe_xO_y@C spheres, with a nominal iron nitrate/C ratio of 3:5. This is much higher than the loading of∼1 wt % in the iron oxide shell−carbon core spheres prepared following the procedure proposed by Titirici et al.[3d] In addition, the Fe_2O_3 loading in the spheres prepared by our method is readily adjustable. By changing the initial nominal iron nitrate/C ratio to 1:5, we were able to synthesize Fe_xO_y@C spheres with an Fe_2O_3 loading of 7.4 wt %. Moreover, it is worthy of note that the carbon source is not limited to glucose in this approach. Fe_xO_y@C spheres identical to those described above were successfully synthesized from fructose and sucrose as carbon sources (Figure S2). Moreover, changing the metal source to cobalt nitrate and nickel nitrate also led to Co_xO_y@C and Ni_xO_y@C spheres, respectively (Figure S3), demonstrating the generality of this approach for the synthesis of metal oxide@C composite materials with this unique microstructure. The occurrence of larger cobalt oxide and nickel oxide nanoparticles in Figure S3 may be associated with the higher hydrothermal temperature of 180 °C for the synthesis of these materials.

The peculiar microstructure makes the as-prepared metal oxide@C spheres very attractive in the fields of electronics, optics, electrochemistry, and catalysis, where the effects are usually size-dependent. Here we invoked the FTS reaction to validate the effectiveness of the confinement of carbonaceous matter on the encapsulated Fe_xO_y nanoparticles. The FTS reaction is the key industrial process for the production of ultraclean transportation fuels, chemicals, and other hydrocarbons from synthesis gas derived from coal, natural gas, or biomass. It has been reported that the particle size of the iron-based catalysts has profound effects on the FTS activity and selectivity.[8]

Prior to the FTS reaction, the Fe_xO_y@C spheres were activated in 5% H_2/Ar at 400 °C for 16 h. Because of the further carbonization of the carbonaceous spheres at higher temperatures, the reduced spheres experienced a slight contraction to a size of ∼5 μm. However, the spherical contour remained unaltered (Figure S4). The particle size of the iron species inside the carbonaceous spheres increased to ∼7 nm (Figure S5a) as a result of the transformation of Fe_xO_y to iron carbides (θ-Fe_3C and χ-$Fe_{2.5}C$) (Figure 3b,c and Table S2).[13] Moreover, because of the further gasification of the carbonaceous matter during the activation process (Figure S6), the porosity of the reduced Fe_xO_y@C spheres was increased (Table S3), ensuring better accessibility of the embedded iron species to the reactants. Figure 4 presents the FTS results over the reduced Fe_xO_y@C spheres. The CO conversion was 86% initially and then decreased to 76% after 70 h on stream, with no further change observed over prolonged reaction times. For comparison, CO

conversion on the carbon nanotube-supported iron catalyst dropped much faster (from 45 to 15%) within 50 h of testing, even at a reaction temperature 50 °C lower than the present case.[14] The normalized activity per gram of Fe for the reduced Fe_xO_y@C spheres is comparable to those of literature iron catalysts (Table S4), which is additional evidence for the accessibility of the iron species in the reduced Fe_xO_y@C spheres to the reactants. Moreover, the selectivities toward olefin and long-chain hydrocarbons (C_5-C_{20}) were high when the reduced Fe_xO_y@C spheres were used as the FTS catalyst and did not undergo significant changes during the whole reaction period (Figure S7). In particular, the C_{5-12} fraction amounted to 40% in the products, and this is better than the values reported to date for iron catalysts without promotion, including the Fe-*in*-CNT, Fe-*out*-CNT, and Fe/activated carbon catalysts.[8d,15]

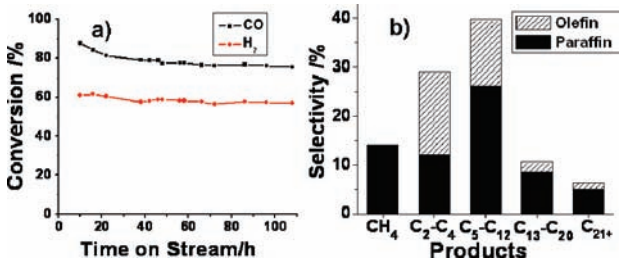

Figure 4. FTS performance over the reduced Fe_xO_y@C spheres. (a) Conversions of CO and H_2 vs time on stream. (b) Hydrocarbon selectivities at 108 h on stream.[16]

The high stability of the reduced Fe_xO_y@C spheres in the FTS reaction is compatible with the TEM observations that the particle size of the iron species was only slightly enlarged from ~7 to ~9 nm after 108 h on stream (Figure S5b), which indicates a confinement effect of the carbonaceous matter on the sintering of the iron carbide nanoparticles during the FTS reaction. On the other hand, the excellent selectivity to C_{5+} hydrocarbons can be attributed to the presence of more iron carbides in the reduced Fe_xO_y@C spheres due to the improved reaction between nanosized Fe_xO_y and the surrounding carbonaceous matter according to the thermodynamic stability of iron carbide, which is beneficial for the production of long-chain hydrocarbons.[17] As shown in Table S2, the iron carbides account for more than 88% of the total amount of iron species in the reduced Fe_xO_y@C spheres. Although a direct correlation was not intended by Chen et al.,[15b] they also identified that the Fe-*in*-CNT catalyst, which had a higher Fe_xC_y/FeO ratio than the Fe-*out*-CNT catalyst, exhibited a higher selectivity to C_{5+} hydrocarbons.

In summary, we have demonstrated a facile and efficient one-pot route for the fabrication of Fe_xO_y@C spheres embedded with highly dispersed iron oxide nanoparticles by hydrothermal treatment of a glucose solution containing iron nitrate at a mild temperature. The catalytic study revealed the remarkable stability and selectivity of the reduced Fe_xO_y@C spheres in the FTS reaction, which clearly exemplifies the confinement effect of the carbonaceous matter on the embedded nanoparticles imparted by the unique microstructure. The surrounding carbonaceous matter facilitated the formation of iron carbides during H_2 activation, which is beneficial for the formation of C_{5+} hydrocarbons, and restricted the aggregation of the iron carbide nanoparticles during the activation and reaction processes. This preparation route is also applicable to a range of other naturally occurring saccharides and metal nitrates. Moreover, by properly tailoring the surface properties of the nanoparticles, this strategy may be extended to the synthesis of other metal oxide@C, metal@C, and zeolite@C materials with this interesting microstructure, which may find important applications as catalysts, adsorbents, sensors, electrodes, and advanced electronic materials in many scientific disciplines.

Acknowledgment. This work was supported by the National Basic Research Program of China (2006CB202502), the NSF of China (20673025, 20703011), the Fok Ying Tong Education Foundation (104022), the NCET, the Science & Technology Commission of Shanghai Municipality (06JC14009, 08DZ2270500), the Beijing Synchrotron Radiation Facility (BSRF), and the Key Laboratory of Nuclear Analysis Techniques, Chinese Academy of Sciences.

Supporting Information Available: Experimental details; XAS, SEM, TEM, thermogravimetric analysis, and N_2 physisorption results; ^{57}Fe Mössbauer parameters; and catalytic data for FTS. This material is available free of charge via the Internet at http://pubs.acs.org.

References

(1) Sun, X. M.; Li, Y. D. *Angew. Chem., Int. Ed.* **2004**, *43*, 597.
(2) Sevilla, M.; Fuertes, A. B. *Chem.—Eur. J.* **2009**, *15*, 4195.
(3) (a) Wang, C. H.; Chu, X. F.; Wu, M. M. *Sens. Actuators, B* **2007**, *120*, 508. (b) Sun, X. M.; Li, Y. D. *Angew. Chem., Int. Ed.* **2004**, *43*, 3827. (c) Li, X. L.; Lou, T. J.; Sun, X. M.; Li, Y. D. *Inorg. Chem.* **2004**, *43*, 5442. (d) Titirici, M. M.; Antonietti, M.; Thomas, A. *Chem. Mater.* **2006**, *18*, 3808.
(4) Sun, X. M.; Li, Y. D. *Langmuir* **2005**, *21*, 6019.
(5) Zhong, Z. Y.; Ho, J.; Teo, J.; Shen, S. C.; Gedanken, A. *Chem. Mater.* **2007**, *19*, 4776.
(6) Parks, G. A. *Chem. Rev.* **1965**, *65*, 177.
(7) (a) Emory, S. R.; Haskins, W. E.; Nie, S. M. *J. Am. Chem. Soc.* **1998**, *120*, 8009. (b) Heiz, U.; Vanolli, F.; Sanchez, A.; Schneider, W. D. *J. Am. Chem. Soc.* **1998**, *120*, 9668. (c) Sun, X. M.; Liu, J. F.; Li, Y. D. *Chem.—Eur. J.* **2006**, *12*, 2039. (d) Zhang, W. M.; Hu, J. S.; Guo, Y. G.; Zheng, S. F.; Zhong, L. S.; Song, W. G.; Wan, L. J. *Adv. Mater.* **2008**, *20*, 1160. (e) Demir-Cakan, R.; Titirici, M. M.; Antonietti, M.; Cui, G. L.; Maier, J.; Hu, Y. S. *Chem. Commun.* **2008**, 3759.
(8) (a) Jung, H. J.; Walker, P. L., Jr.; Vannice, A. *J. Catal.* **1982**, *75*, 416. (b) Boudart, M.; McDonald, M. A. *J. Phys. Chem.* **1984**, *88*, 2185. (c) Jones, V. K.; Neubauer, L. R.; Bartholomew, C. H. *J. Phys. Chem.* **1986**, *90*, 4832. (d) Guczi, L.; Stefler, G.; Geszti, O.; Koppány, Zs.; Kónya, Z.; Molnár, É.; Urbán, M.; Kiricsi, I. *J. Catal.* **2006**, *244*, 24.
(9) (a) Bezemer, G. L.; Bitter, J. H.; Herman, P. C. E.; Kuipers, H. P. C.; Oosterbeek, H.; Holewijn, J. E.; Xu, X. D.; Kapteijn, F.; van Dillen, A. J.; de Jong, K. P. *J. Am. Chem. Soc.* **2006**, *128*, 3956. (b) Khodakov, A. Y.; Chu, W.; Fongarland, P. *Chem. Rev.* **2007**, *107*, 1692. (c) Sietsma, J. R. A.; Meeldijk, J. D.; den Breejen, J. P.; Versluijs-Helder, M.; van Dillen, A. J.; de Jongh, P. E.; de Jong, K. P. *Angew. Chem., Int. Ed.* **2007**, *46*, 4547. (d) Xiao, C. X.; Cai, Z. P.; Wang, T.; Kou, Y.; Yan, N. *Angew. Chem., Int. Ed.* **2008**, *47*, 746. (e) Kang, J. C.; Zhang, S. L.; Zhang, Q. H.; Wang, Y. *Angew. Chem., Int. Ed.* **2009**, *48*, 2565.
(10) (a) Cui, X. J.; Antonietti, M.; Yu, S. H. *Small* **2006**, *2*, 756. (b) Wang, C. L.; Ma, D.; Bao, X. H. *J. Phys. Chem. C* **2008**, *112*, 17596.
(11) (a) Tshuva, E. Y.; Lippard, S. J. *Chem. Rev.* **2004**, *104*, 987. (b) Zhao, M.; Helms, B.; Slonkina, E.; Friedle, S.; Lee, D.; DuBois, J.; Hedman, B.; Hodgson, K. O.; Fréchet, J. M. J.; Lippard, S. J. *J. Am. Chem. Soc.* **2008**, *130*, 4352.
(12) (a) Yu, D. H.; Aihara, M.; Antal, M. J., Jr. *Energy Fuels* **1993**, *7*, 574. (b) Minowa, T.; Zhen, F.; Ogi, T. *J. Supercrit. Fluids* **1998**, *13*, 253. (c) Seri, K.; Sakaki, T.; Shibata, M.; Inoue, Y.; Ishida, H. *Bioresour. Technol.* **2002**, *81*, 257.
(13) Mahajan, D.; Gütlich, P.; Ensling, J.; Pandya, K.; Stumm, U.; Vijayaraghavan, P. *Energy Fuels* **2003**, *17*, 1210.
(14) van Steen, E.; Prinsloo, F. F. *Catal. Today* **2002**, *71*, 327.
(15) (a) Jambor, J. L.; Dutrizac, J. E. *Chem. Rev.* **1998**, *98*, 2549. (b) Chen, W.; Fan, Z. L.; Pan, X. L.; Bao, X. H. *J. Am. Chem. Soc.* **2008**, *130*, 9414.
(16) Prior to the FTS reaction, the Fe_xO_y@C sample (2.0 g) diluted with quartz powder was reduced in situ in 5% H_2/Ar (50 mL min^{-1}) for 16 h at 400 °C (ramping rate 2 °C min^{-1}). Catalytic testing was conducted in 2:1 (v/v) H_2/CO (flow rate 16.7 mL min^{-1}, 270 °C, 2.0 MPa) in a tubular fixed-bed reactor (10 mm i.d.).
(17) Bukur, D. B.; Nowicki, L.; Manne, R. K.; Lang, X. S. *J. Catal.* **1995**, *155*, 366.

JA906370B